Effect of Particle Connectivity on Heat Transfer in Granular Materials Using Complex Networks

Wenbin Fei, Guillermo A. Narsilio(✉), and Mahdi M. Disfani

Department of Infrastructure Engineering, The University of Melbourne, Melbourne, Australia
narsilio@unimelb.edu.au

Abstract. Effective thermal conductivity (ETC) is affected by interparticle connectivity in granular geomaterials, which can be characterised by coordination number. Complex network theory can be used to identify "features" that are also able to quantify the particle connectivity. However, this new class of variables have not been used to study the effective thermal conductivity in real sands. An advantage of some network features is that they can simultaneously consider both the particle connectivity and contact quality by adding a contact area or thermal conductance as a weight to connectivity variables. In this paper, weighted closeness centrality extracted from the computed tomography images of five natural sands is shown to be a good predictor of ETC of the sands.

Keywords: Thermal conductivity · Complex network theory · Heat transfer · Microstructure

1 Introduction

Heat transfer progress is essential in engineering applications such as geothermal engineering (Rohsenow et al. 1985), radioactive waste disposal (Bergles et al. 1981) and CO_2 geological storage (Fei et al. 2015). Since effective thermal conductivity (ETC) is a crucial parameter indicating how easily heat travels through the geomaterials, predicting ETC accurately affects the cost evaluation and the feasibility of these projects.

The difficulty of accurately predicting ETC of geomaterials (e.g. sands) comes from their inherent complexity since the internal grains varies in size, shape and dispersibility. In a dry granular material, the heat mainly transfers through the interparticle contact (Yun and Santamarina 2008). Hence, it is important to quantify the interparticle connectivity and contact quality. Porosity is a parameter widely used in predicting ETC because it hints the fraction of the solid volume to the total volume of a material and the interparticle connectivity. However, this indirect characterisation of interparticle connectivity may limit the availability of porosity-dependent models to materials with a specific range of porosity.

Alternatively, the coordination number is a widely used parameter to measure the interparticle connectivity in granular materials (Fonseca et al. 2013, Liu et al. 2011).

M. Barla et al. (Eds.): IACMAG 2021, LNCE 126, pp. 1002–1009, 2021.
https://doi.org/10.1007/978-3-030-64518-2_119

Other attempts of directly quantifying interparticle connectivity include using Voronoi tessellation (Cheng et al. 1999) and classifying materials into typical regular structures (Siu and Lee 2000). However, these studies worked on sphere packings rather than real sands. Fei et al. (2019) applied contact network to present real sands by scanning sands with computed tomography (CT) technology, and then creating a node for each grain in the sand and generating an edge for each interparticle contact. Based on the contact networks, three contact network features were calculated to quantify the interparticle connectivity. Together with particle shape descriptors used for indicating contact quality, they were used to predict ETC well in real sands. However, two questions raised from this work: (a) how to unify the interparticle connectivity and contact quality into a single parameter, and (b) could the contribution of the small gap between neighbouring particles be also considered in the single parameter.

The present paper aims to address the first question by adding an interparticle contact area as weight at each edge in the contact networks and then calculating a network parameter (or 'feature') know as closeness centrality. To settle the second question, the contact networks were extended to thermal networks by creating new edges for the small gaps between neighbouring particles and then thermal conductance was added to each edge as a weight. This paper also investigates the relationship between the weighted closeness centrality and ETC in five real sands.

2 Sample Preparation and Measurements

Five sands with distinct shapes were selected. Each of the sands was air-pluviated in a cylinder with a diameter of 25 mm and a height of 25 mm to ensure the homogeneity of the specimen. The prepared specimens were then sent to the Australian Synchrotron to obtain CT images with a voxel size of 13 μm as shown in Fig. 1. The glass beads are almost spheres. The grains in Ottawa sand are not as spherical but have round corners. In contrast, grains in angular sand are more irregular than those in Ottawa sand, and some grains have sharp corners. Crushed schist A has grains with a more elongated shape and rough surface. The grains in crushed schist B are most irregular among the five sands, more than half of the grains are elongated and platy. The D_{50} and particle size range of each sand was measured by conducting sieve analysis, the results are shown in Table 1.

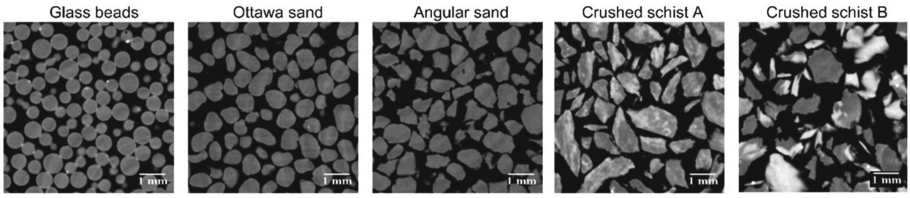

Fig. 1. CT images of the selected five sands (Fei et al. 2019)

Table 1. Particle size of the sands in this paper

Sand	D_{50} (mm)	Min particle diam. (mm)	Max particle diam. (mm)
Glass beads	0.60	0.50	0.70
Ottawa sand	0.73	0.60	0.85
Angular sand	0.89	0.60	1.18
Crushed schist rock A	0.84	0.50	1.18
Crushed schist rock B	0.84	0.50	1.18

Each sand was also air-pluviated in a cylinder with a diameter of 50 mm and a height of 120 mm to minimise differences between this specimen and the CT samples. Then the ETC of the specimen was measured using a thermal needle probe following standard procedures (ASTM D5334–14 2014). The probe has a diameter of 24 mm and length of 100 mm, its diameter is larger than the D_{50} of the sand as shown in Table 1 to ensure that many grains are touched by the probe (to enhances the accuracy of the measured ETC).

3 Image Processing, Network Construction and Network Features

3.1 Image Processing

From the random locations of the scanned image stacks of each sand (Fig. 1), four cubic subsamples with an edge length of 4.5 mm were cropped. Otsu threshold segmentation was chosen to separate the solid phases (grey in Fig. 2(a)) and the void phases (black in Fig. 2(a)) in CT images and to achieve binary images, i.e. solid phase in black while the void phase in white. Since each grain corresponds to a node in a network., the solids were required to be separated into individuals by removing the contacts. A watershed segmentation plugin MorphoLibJ (Legland et al. 2016) was implemented on the binary image stack (Fig. 2(b)) and the result is shown in Fig. 2(c). Meanwhile, each individual grain was labelled with a unique ID and rendered with random colours.

3.2 Network Construction

Based on the labelled watershed segmented images, contact network was built first. As shown in Fig. 3(a), a node was created in the centroid of each grain and an edge was created to present each interparticle contact. The interparticle contact was detected by adding all the shared boundary voxels between neighbouring grains together, details of the procedure can be found in Fei et al. (2019). These shared boundary voxels were also used to compute the interparticle contact area and thermal conductance later. A thermal network is an extension of the contact network by considering the heat transfer through small gaps between particles. The small gap was named ‘near-contact’ in the present work and it exists next to the interparticle contact and also solely between

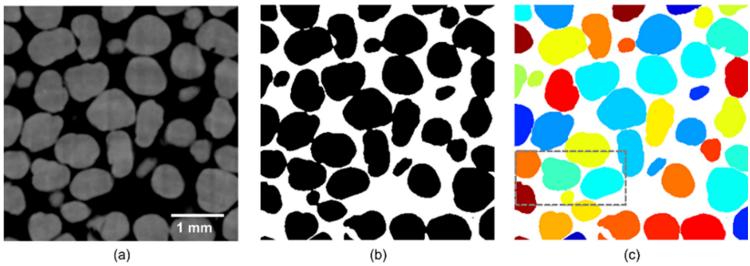

Fig. 2. Image processing procedures of a single image for example. a) CT image, (b) binary image after threshold segmentation, (c) separate solids after watershed segmentation and with unique IDs were rendered with random colours.

neighbouring particles as shown in Fig. 3(b). Hence, these near-contacts were identified by checking if the shortest distance between boundary voxels on each side of the gap smaller than half the average particle radius (Fei et al. 2019).

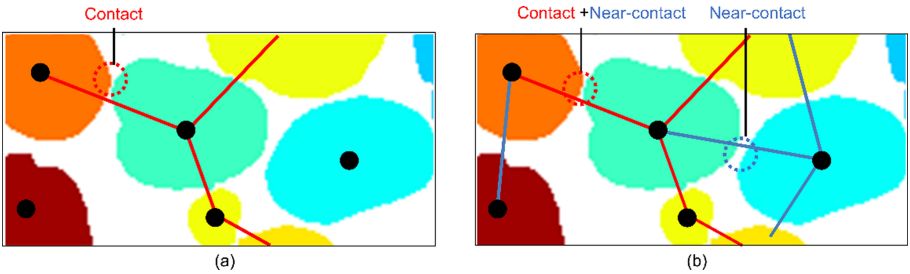

Fig. 3. Constructing contact network and thermal network. The edges in red represent interparticle contact while the edges in blue represent the near-contacts (small gaps that heat could transfer through) [Detail from dashed rectangle in Fig. 2-c]

3.3 Network Feature(s)

Particle connectivity variables are scarce with only 'coordination number' being widely used in geotechnical engineering. Recently, network features were applied to granular materials to investigate the mechanical stability (Walker and Tordesillas 2010) and fluid flow (van der Linden et al. 2016). In this paper, closeness centrality was selected to quantify the particle connectivity and its correlation with ETC was also studied. In a network, closeness centrality measures the closeness of a certain node to others. As shown in Eq. 1 (Freeman 1978), a node i in a node set V from a network can be calculated as the reciprocal of the total shortest path d(i,j) between the node i and another node j. Closeness centrality was also normalised using the parameter $\beta = |V|-1$ which is the number of reachable nodes in a network to mitigate the influence of particle number in different samples. Compared with coordination number focusing on the local information of a particle and porosity generalising the void/solid percentage at

the sample scale, the closeness centrality is a mesoscale parameter containing more microstructural information since it covers more than one node/grain in the sample.

$$[G^*]_C(i) = \beta \left[\sum_{j=1}^{|V|-1} d(i,j) \right]^{-1} \tag{1}$$

where $[G^*]_C$ is a unified parameter, $[G^C]_C$ means that closeness centrality from the contact network while $[G^T]_C$ refers to the feature from the thermal network.

Additionally, this mesoscale feature could characterise contact quality at the same time. In a contact network, the contact quality is related to the interparticle contact area which can be calculated using the shared voxels between neighbouring particles. Since the near-contact was identified using the shortest length between the boundary voxels on each side of the near-contact, the contact quality in the thermal network was quantified with thermal conductance. Three types of cylinders including particle cylinder (heat transfer through solid), contact cylinder (heat transfer through interparticle contact), and gap cylinder (heat transfer through near-contact) (Fei et al. 2019) were used to compute the contact quality at the red edge and blue edge in Fig. 3(b). For a pure near-contact, each shortest link i with length L was considered as a pipe with cross-section area A. Then its thermal conductance C^{gap} can be calculated as Eq. 2. Next, this gap thermal conductance with the particle thermal conductance of the two neighbouring solids could be harmonically averaged and added as the weight to the blue edge in the thermal network (Fig. 3(b)). Similarly, the thermal conductance at the red edge could also be calculated using the harmonic average of the thermal conductance in the two neighbouring particles, the sum of contact thermal conductance and gap thermal conductance (Fei et al. 2019).

$$C^{gap} = \sum_i \frac{\lambda_v A}{L(i)} \tag{2}$$

where λ_V is the thermal conductivity of the void phase, A is equal to the surface area of a pixel.

After contact area or thermal conductance were added to the edges of the network, the closeness centrality had a unit of (m^2) or (W/K). Hence, the weighted closeness centrality $[G^C]_C$ from the contact network was divided by $D_{50}{}^2$ and the weighted closeness centrality $[G^T]_C$ from thermal network was divided by $\lambda_{solid} \cdot D_{50}$ to make the feature dimensionless.

4 Finite Element Simulation

Finite element method was employed to simulate the heat transfer and calculate the ETC following the framework introduced by Narsilio et al. (2009). The representative element volume (REV) has a dimension of 4.5 mm × 4.5 mm × 4.5 mm. The thermal conductivity of the solid was set as 3 W/(mK) while the thermal conductivity of the air in the void was 0.025 W/(mK). The temperature on the top boundary of the domain

was set as 293 K which was 1 K larger than that on the bottom boundary, whereas other side boundaries were insulated.

For each sand, the calculated ETC of the four selected subsamples together with experimental results and ETC from literature (Narsilio et al. 2010, Yun and Santamarina 2008) are shown in Fig. 4. The ETC decreases with the increase of porosity and the correlation coefficient is as high as 0.93. However, the change of ETC becomes stagnant when the porosity is larger than 0.5, which indicates the porosity-dependent models may only available for dry sands within a certain range of porosity. The calculated ETC is larger than that from thermal needle tests, which may be because of the errors during experiments and the incorrect recognition of partially filled voxels in CT images as solids. The second error could be reduced if CT images with higher resolution were achieved. High resolution images could also identify the roughness on the particle surface, but attention needs to be paid on balancing image resolution and sample size.

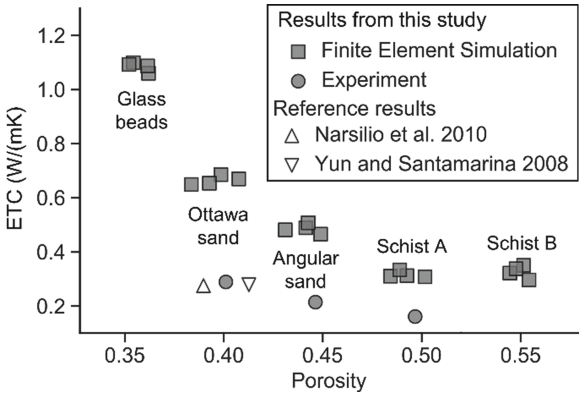

Fig. 4. The numerically calculated ETC compared with experimental results.

5 Relationship Between Closeness Centrality and ETC

After calculating the closeness centrality (from both contact network and thermal network) and the ETC of each sand, their correlations are shown in Fig. 5. As closeness centrality $[G^*]_C$ measures the average distance between each two grains in a sand, an increase in $[G^*]_C$ indicates that grains are closer to each other and the sample has better connectivity. Hence, heat will be more natural to transfer and ETC in the sample tends to be larger. Indeed, Fig. 5(a) presents that the closeness centrality $[G^G]_C$ from contact network has an increasing linear relationship with a correlation coefficient R^2 of 0.86. Even though the R^2 is not as high as the correlation between porosity and ETC, this linear relationship is simpler, and it overcomes the stagnant tail in Fig. 4. A linear fit (Eq. 3) between closeness centrality $[G^T]_C$ from contact network and ETC is found:

$$\frac{\lambda_{eff}}{\lambda_{solid}} = 83.6\left[G^T\right]_C - 0.70 \tag{3}$$

A quadratic polynomial may have a better correlation coefficient. Compared with the data distribution in Fig. 5(a) clusters at the two ends, considering the contribution of near-contact to heat transfer enables the closeness centrality distributes more evenly in Fig. 5(b) even though the R^2 is slightly smaller (0.83). Therefore, network features can be good predictors to ETC. If considering the effect of heat convection in wet sample or heat radiation when the sample in a high temperature, the contribution of small gaps between particles may be more important, resulting in the more significant importance of the thermal network feature.

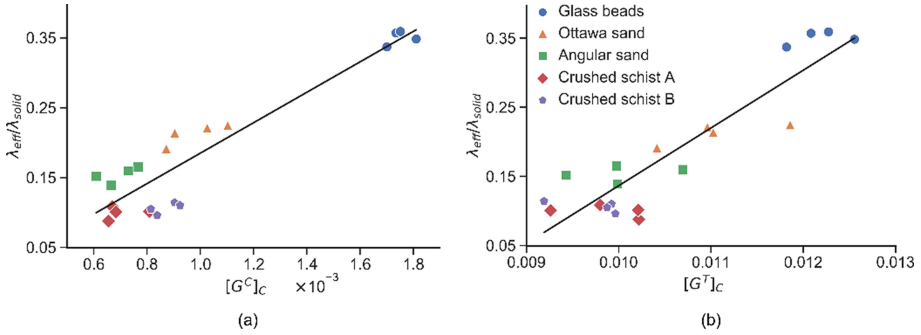

Fig. 5. The correlation between ECT and (a) closeness centrality $\left[G^C\right]_C$ from contact network, and (b) closeness centrality $\left[G^T\right]_C$ from the thermal network.

6 Conclusions

In the present study, weighted closeness centrality from both the contact network and the thermal network was calculated based on CT images of five real sands. The weighted closeness centrality considers both particle connectivity and contact quality. The contact quality is related to the contact area in contact networks and thermal conductance in thermal networks. The good correlation between the weighted closeness centrality and ETC indicates that network features have the potential of predicting ETC accurately. Future work may investigate the relationship between other types of network features (e.g. node betweenness centrality, edge betweenness centrality, etc.) and ETC.

Acknowledgements. The activity presented in the paper is supported by the Melbourne Research Scholarship offered by The University of Melbourne in Australia. The authors also thank Dr Anton Maksimenko and the other academics at Australian Synchrotron, Victoria, Australia for supporting us in obtaining images via CT imaging and medical beamline (IMBL).

References

Astm D5334-14. Standard Test Method for Determination of Thermal Conductivity of Soil and Soft Rock by Thermal Needle Probe Procedure. West Conshohocken, PA, ASTM (2014)

Bergles, A.E., Collier, J., Delhaye, J.M., Hewitt, G., Mayinger, F.: Two-phase flow and heat transfer in the power and process industries. Hemisphere New York (1981)

Cheng, G., Yu, A., Zulli, P.: Evaluation of effective thermal conductivity from the structure of a packed bed. Chem. Eng. Sci. **54**(19), 4199–4209 (1999)

Fei, W., Narsilio, G.A., Van Der Linden, J.H., Disfani, M.M.: Quantifying the impact of rigid interparticle structures on heat transfer in granular materials using networks. Int. J. Heat Mass Transf. **143**, 118514 (2019)

Fei, W., Li, Q., Wei, X., Song, R., Jing, M., Li, X.: Interaction analysis for CO2 geological storage and underground coal mining in Ordos Basin China. Eng. Geology **196**, 194–209 (2015)

Fonseca, J., O'sullivan, C., Coop, M.R., Lee, P.: Quantifying the evolution of soil fabric during shearing using directional parameters. Géotechnique **63**(6), 487–499 (2013)

Freeman, L.C.: Centrality in social networks conceptual clarification. Soc. Netw. **1**(3), 215–239 (1978)

Legland, D., Arganda-Carreras, I., Andrey, P.: MorphoLibJ: integrated library and plugins for mathematical morphology with ImageJ. Bioinformatics **32**(22), 3532–3534 (2016)

Liu, A., Nagel, S., Van Saarloos, W., Wyart, M.: The jamming scenario-an introduction. In: Dynamical Heterogeneities in Glasses, Colloids, and Granular Media. Oxford Univerity Press (2011)

Narsilio, G.A., Buzzi, O., Fityus, S., Yun, T.S., Smith, D.W.: Upscaling of navier-stokes equations in porous media: theoretical, numerical and experimental approach. Comput. Geotech. **36**(7), 1200–1206 (2009)

Narsilio, G.A., Kress, J., Yun, T.S.: Characterisation of conduction phenomena in soils at the particle-scale: finite element analyses in conjunction with synthetic 3D imaging. Comput. Geotech. **37**(7), 828–836 (2010)

Rohsenow, W.M., Hartnett, J.P., Ganic, E.N.: Handbook of Heat Transfer Applications, p. 273. McGraw-Hill Book Co., New York (*1985*)

Siu, W., Lee, S.K.: Effective conductivity computation of a packed bed using constriction resistance and contact angle effects. Int. J. Heat Mass Transfer **43**(21), 3917–3924 (2000)

Van Der Linden, J.H., Narsilio, G.A., Tordesillas, A.: Machine learning framework for analysis of transport through complex networks in porous, granular media: a focus on permeability. Phys. Rev. E **94**(2), 022904 (2016)

Walker, D.M., Tordesillas, A.: Topological evolution in dense granular materials: a complex networks perspective. Int. J. Solids Struct. **47**(5), 624–639 (2010)

Yun, T.S., Santamarina, J.C.: Fundamental study of thermal conduction in dry soils. Granular Matter **10**(3), 197 (2008)